INTERNATIONAL JOURNAL FOR NUMERICAL METHODS IN FLUIDS
Int. J. Numer. Meth. Fluids 2009; **59**:1241–1258
Published online 17 July 2008 in Wiley InterScience (www.interscience.wiley.com). DOI: 10.1002/fld.1865

Efficient computation of mean drag for the subcritical flow past a circular cylinder using general Galerkin G2

J. Hoffman*, †

School of Computer Science and Communication, KTH, SE-10044 Stockholm, Sweden

SUMMARY

General Galerkin (G2) is a new computational method for turbulent flow, where a stabilized Galerkin finite element method is used to compute approximate weak solutions to the Navier–Stokes equations directly, without any filtering of the equations as in a standard approach to turbulence simulation, such as large eddy simulation, and thus no Reynolds stresses are introduced, which need modelling. In this paper, G2 is used to compute the drag coefficient c_D for the flow past a circular cylinder at Reynolds number $Re=3900$, for which the flow is turbulent. It is found that it is possible to approximate c_D to an accuracy of a few percent, corresponding to the accuracy in experimental results for this problem, using less than 10^5 mesh points, which makes the simulations possible using a standard PC. The mesh is adaptively refined until a stopping criterion is reached with respect to the error in a chosen output of interest, which in this paper is c_D. Both the stopping criterion and the mesh-refinement strategy are based on *a posteriori* error estimates, in the form of a space–time integral of residuals times derivatives of the solution of a dual problem, linearized at the approximate solution, and with data coupling to the output of interest. Copyright © 2008 John Wiley & Sons, Ltd.

Received 31 August 2005; Revised 12 May 2008; Accepted 25 May 2008

KEY WORDS: adaptive DNS/LES; general Galerkin (G2); adaptive finite element method; duality; *a posteriori* error estimate; turbulence; large eddy simulation (LES); direct numerical simulation (DNS); circular cylinder

1. INTRODUCTION

The flow past a circular cylinder is probably one of the best documented bluff body flows, investigated extensively both experimentally and computationally. For an overview of the underlying physics of this problem, including many results, we refer to [1, 2].

In this paper we focus on Reynolds numbers $Re=100$ and 3900, with the Reynolds number being based on the cylinder diameter D. For $Re=100$, the flow is two dimensional, with a

*Correspondence to: J. Hoffman, School of Computer Science and Communication, KTH, SE-10044 Stockholm, Sweden.
†E-mail: jhoffman@nada.kth.se

wake shedding alternating vortices in a regular manner, referred to as a *von Kármán vortex street*.

For $Re=3900$, we still have vortex shedding, but now the flow is three dimensional, and we have a large turbulent wake attached to the cylinder. In the case of the laminar flow at $Re=100$, computational approximation is straightforward by discretizing the Navier–Stokes (NS) equations, for which there are various well-understood approaches, such as finite element methods or finite volume methods.

For turbulent flow, as in the turbulent wake behind the cylinder at $Re=3900$, the situation is less clear. For computational simulation of turbulent flow, there are several issues to be considered: (i) to resolve all the physical scales in a *direct numerical simulation* (DNS) of the NS equations, the number of spatial mesh points needed may be estimated to be of the order $Re^{9/4}$, which thus makes DNS impossible for high Re and (ii) turbulent flow is a *chaotic system* [3] in the sense that pointwise output, such as the velocity at a certain point at a given time in the turbulent wake, is impossible to compute to any tolerance of interest, due to the extremely high sensitivity to perturbations with respect to pointwise output, whereas certain mean value outputs are less sensitive and may be determined up to a tolerance of interest.

Thus, for high Re turbulent flow we cannot afford to resolve all the physical scales in the problem and even if we could, we would not be able to obtain pointwise accuracy, due to the extreme pointwise sensitivity to perturbations in a turbulent flow, which would make a DNS solution pointwise wrong. On the other hand, there are aspects of a turbulent flow that are less sensitive to perturbations, so that certain mean value output, such as mean values in time of drag and lift forces, for example, may be approximated from a DNS solution to an accuracy of say a few percent.

The traditional approach to get around the impossibility (i) of DNS at high Reynolds numbers is to seek to approximate some average of the turbulent flow field. One such approach is *large eddy simulation* (LES), where the NS equations are averaged, using a filter operator, resulting in a new set of equations for the filtered flow variables, involving the so-called *Reynolds stresses*, due to filtering of the non-linear term in the NS equations. The Reynolds stresses depend on the unfiltered velocity field and thus need to be modelled in terms of the filtered velocity field in a *turbulence model*, or *subgrid model*, which is referred to as the *closure problem* of turbulence. Many subgrid models for LES have been proposed, typically having a dissipative nature, and we refer to [4] for an overview of LES and subgrid modelling. Mean value output is then computed by postprocessing the LES solution.

LES is a popular method, and several computational studies for the flow past a circular cylinder at $Re=3900$ have been performed using LES, see e.g. [5–7]. Although, there are several problems with LES, in particular: (i) the closure problem is not solved; many different subgrid models are being used, and the models seem to be problem dependent and highly influenced by the numerical method used, and (ii) the definition of the LES solution close to boundaries is not always clear [8].

G2 is an adaptive stabilized Galerkin finite element method. In [9, 10] G2 is introduced as an adaptive computational method for turbulent flow, where a chosen mean value output $M(\cdot)$ is computed to a specified tolerance TOL, using a minimal number of degrees of freedom from the NS equations. No filtering is used, and thus the introduction of Reynolds stresses is avoided, and the closure problem (i) of LES is circumvented, in the sense that no Reynolds stresses need to be modelled, which greatly simplifies turbulence simulation. The complication (ii) of LES is also avoided.

DOI: 10.1002/fld

We sometimes refer to G2 for turbulent flow as *adaptive DNS/LES*, where adaptively some parts of the flow are fully resolved in a DNS, whereas other parts are left underresolved in a LES with the stabilization in G2 acting as a simple subgrid model.

G2 is based on *a posteriori error estimates*, where the output sensitivity information is obtained by computational approximation of an associated *dual problem*, linearized at an approximate G2 solution $\hat{U}$, with data coupling to the output of interest. We thus solve the minimization problem: *Find a mesh with a minimal number of degrees of freedom*, *such that*

$$|M(\hat{u}) - M(\hat{U})| \leqslant \mathrm{TOL} \tag{1}$$

where $\hat{u}$ is a representative solution to the NS equations, such that $M(\hat{u})$ is the target value for the output $M(\cdot)$. In this paper, we only consider adaptive refinement of the spatial mesh, with the time step being proportional to the smallest cell diameter in the mesh. The details in the definition of $\hat{u}$ are related to the question of *output uniqueness* of solutions to the NS equations [3]. For our purposes in this paper, it suffices to consider $\hat{u}$ as a solution to the NS equations, such that $M(\hat{u})$ is the target output that we try to approximate.

Depending on the output we want to compute, the complexity of the flow, and the computer resources we have available, we may find it impossible to compute the output to the desired accuracy. A way out of this problem is then either to seek more powerful computer resources, settle for a less sharp tolerance, or to aim for a less demanding output.

A key to the success of G2 is that dual solutions corresponding to certain mean value outputs are stable with respect to the linearization at $\hat{U}$, and thus that the *a posteriori* output error estimate can be trusted. That is, small perturbations in $\hat{U}$ result in small changes in the dual solution, which makes it possible to approximate $\hat{u}$ by $\hat{U}$ in the linearization of the dual problem. Questions of computability, predictability, and uniqueness of turbulent solutions to the NS equations are investigated in [3], where the stability of the dual solution under perturbations from linearization errors is investigated computationally for a number of turbulent flow problems.

For an overview of adaptive finite element methods including references, we refer to the survey articles [11–13]. For incompressible flow, applications of adaptive finite element methods based on duality have been used to compute quantities of interest such as the drag force for two-dimensional stationary benchmark problems in [14, 15]. In [16] time-dependent problems in three dimensions are first considered, and the extension of this framework to LES is investigated in [17]. The generalization to turbulent flow is first presented in [9, 10], with applications to flow around a surface mounted cube, and a square cylinder, and in [3] the basis for this approach for turbulent flow in general is investigated.

Owing to the possibilities offered by G2, it is important to assess the method for available benchmark problems. In [10] the flow around a surface mounted cube and the flow around a square cylinder are investigated, and in this paper we apply G2 to the problem of computing the mean drag coefficient c_{D} for a circular cylinder at $Re = 3900$. The circular geometry of the cylinder makes this a much more challenging problem than the problems considered in [10] with square geometries. The reason for this is that for the square geometries, the separation of the flow is determined by the geometry, with separation at the upstream edges. On the other hand, for the problem considered in this paper, the separation depends on the Reynolds number.

We present results showing that we are able to compute c_{D} to an accuracy of a few percent, corresponding to the accuracy in experimental results, using less than 10^5 mesh points in space. This is a very low number of mesh points, compared with what is generally assumed to be necessary

DOI: 10.1002/fld

for accurate prediction of drag for this problem. Of course, the number of mesh points is not the only factor in determining the overall computational cost. But in general few mesh points are desirable, and we find here that we are able to use a standard PC for advanced turbulence simulations.

Apart from being able to approximate c_D, we are able to capture the correct *Strouhal number St* and pressure distribution on the cylinder. We also compute c_D for the corresponding flow at $Re=100$, illustrating differences in the solution as well as in the adaptive algorithm, compared with the flow at $Re=3900$.

In this paper we use computational meshes that do not change with time, and we use a fixed time step size for each mesh, proportional to the smallest cell diameter.

In Sections 2–5 we recall the discretization of the incompressible NS equations using G2, and the adaptive algorithm for the computation of the drag coefficient. In Section 6 we present the computational model used, and in Sections 7–9 we present computational results.

2. THE NS EQUATIONS

The incompressible NS equations expressing conservation of momentum and incompressibility of a unit density Newtonian fluid with constant kinematic viscosity $\nu>0$ enclosed in a volume Ω in $\mathbb{R}^3$ (where we assume that Ω is a polygonal domain) with homogeneous Dirichlet boundary conditions take the form: Find $\hat{u}=(u,p)$ such that

$$\begin{aligned} \dot{u}+(u\cdot\nabla)u-\nu\Delta u+\nabla p &= f \quad \text{in } \Omega\times I \\ \nabla\cdot u &= 0 \quad \text{in } \Omega\times I \\ u &= 0 \quad \text{on } \partial\Omega\times I \\ u(\cdot,0) &= u_0 \quad \text{in } \Omega \end{aligned} \tag{2}$$

where $u(x,t)=(u_i(x,t))$ is the *velocity* vector; $p(x,t)$ is the *pressure* of the fluid at (x,t); and f, u_0, $I=(0,T)$ are given driving force, initial data and time interval, respectively. The quantity $\nu\Delta u-\nabla p$ represents the total fluid force and may alternatively be expressed as

$$\nu\Delta u-\nabla p=\operatorname{div}\sigma(u,p) \tag{3}$$

where $\sigma(u,p)=(\sigma_{ij}(u,p))$ is the *stress tensor*, with components $\sigma_{ij}(u,p)=2\nu\varepsilon_{ij}(u)-p\delta_{ij}$, composed of the *stress deviatoric* $2\nu\varepsilon_{ij}(u)$ with zero trace and an isotropic pressure: here $\varepsilon_{ij}(u)=(u_{i,j}+u_{j,i})/2$ is the *strain rate tensor*, with $u_{i,j}=\partial u_i/\partial x_j$, and δ_{ij} is the usual Kronecker delta, the indices i and j ranging from 1 to 3. We assume that (2) is normalized so that both the reference velocity and typical length scale are equal to one. The Reynolds number *Re* is then equal to ν^{-1}.

3. DISCRETIZATION: cG(1)cG(1)

The cG(1)cG(1) method is a variant of the *general Galerkin G2 method* [3], using the continuous Galerkin method cG(1) in time. With cG(1) in time, the trial functions are continuous piecewise linear and the test functions are piecewise constant. cG(1) in space corresponds to both test

DOI: 10.1002/fld

functions and trial functions being continuous piecewise linear. Let $0=t_0<t_1<\cdots<t_N=T$ be a sequence of discrete time steps with associated time intervals $I_n=(t_{n-1},t_n]$ of length $k_n=t_n-t_{n-1}$ and space–time slabs $S_n=\Omega\times I_n$, and let $W^n\subset H^1(\Omega)$ be a finite element space consisting of continuous piecewise linear functions on a mesh $\mathscr{T}_n=\{K\}$ of mesh size $h_n(x)$ with W_w^n the functions $v\in W^n$ satisfying the Dirichlet boundary condition $v|_{\partial\Omega}=w$.

We seek $\hat{U}=(U,P)$, continuous piecewise linear in space and time; the cG(1)cG(1) method for the NS equations (2) with homogeneous Dirichlet boundary conditions reads: For $n=1,\ldots,N$, find $(U^n,P^n)\equiv(U(t_n),P(t_n))$ with $U^n\in V_0^n\equiv[W_0^n]^3$ and $P^n\in W^n$, such that

$$\begin{aligned}&((U^n-U^{n-1})k_n^{-1}+\bar{U}^n\cdot\nabla\bar{U}^n,v)+(2\nu\varepsilon(\bar{U}^n),\varepsilon(v))-(P^n,\nabla\cdot v)\\&\quad+(\nabla\cdot\bar{U}^n,q)+\mathrm{SD}_\delta(\bar{U}^n,P^n;v,q)=(f,v)\quad\forall\hat{v}=(v,q)\in V_0^n\times W^n\end{aligned}\tag{4}$$

where $\bar{U}^n=\frac{1}{2}(U^n+U^{n-1})$, with the stabilizing term

$$\mathrm{SD}_\delta(\bar{U}^n,P^n;v,q)\equiv(\delta_1(\bar{U}^n\cdot\nabla\bar{U}^n+\nabla P^n-f),\bar{U}^n\cdot\nabla v+\nabla q)+(\delta_2\nabla\cdot\bar{U}^n,\nabla\cdot v)$$

with $\delta_1=\frac{1}{2}(k_n^{-2}+|U|^2h_n^{-2})^{-1/2}$ in the convection-dominated case $\nu<\bar{U}^nh_n$ and $\delta_1=\kappa_1h_n^2$ otherwise, $\delta_2=\kappa_2h_n$ if $\nu<\bar{U}^nh_n$ and $\delta_2=\kappa_2h_n^2$ otherwise, with κ_1 and κ_2 being positive constants of unit size (in this paper, we have $\kappa_1=\kappa_2=1$), and

$$(v,w)=\sum_{K\in\mathscr{T}_n}\int_K v\cdot w\,\mathrm{d}x$$

$$(\varepsilon(v),\varepsilon(w))=\sum_{i,j=1}^3(\varepsilon_{ij}(v),\varepsilon_{ij}(w))$$

We note that the viscous term $(2\nu\varepsilon(U),\varepsilon(v))$ may alternatively occur in the form $(\nu\nabla U,\nabla v)=\sum_{i=1}^3(\nu\nabla(U)_i,\nabla v_i)$. In the case of Dirichlet boundary conditions, the corresponding variational formulations are equivalent, but not so in the case of Neumann boundary conditions. If we have Neumann boundary conditions, we use the standard technique to apply these boundary conditions weakly.

4. COMPUTATION OF DRAG

An alternative representation of the drag of a body in a fluid is presented in [15] using a volume integral, which is shown to be more accurate than the standard representation in terms of a surface integral. The volume integral takes the following form:

$$N(\sigma(\hat{u}))=\frac{1}{|I|}\int_I(\dot{u}+u\cdot\nabla u-f,\Phi)-(p,\nabla\cdot\Phi)+(2\nu\varepsilon(u),\varepsilon(\Phi))+(\nabla\cdot u,\Theta)\,\mathrm{d}t\tag{5}$$

where Φ is a function defined in the fluid volume Ω, being equal to a unit vector along the channel in the direction of the flow on Γ_0, the surface of the body in contact with the fluid, and zero on the remaining part of the boundary $\Gamma_1=\partial\Omega\setminus\Gamma_0$ of the fluid volume. The representation (5) is independent of Θ and the particular extension of Φ away from the boundary.

DOI: 10.1002/fld

Here we think of $\hat{u}=(u, p)$ as being a solution to (2) in the fluid volume Ω surrounding the body (using suitable boundary conditions as specified below), defining the target output $N(\sigma(\hat{u}))$, with sufficient regularity for (5) to be well defined.

We can to compute an approximation of the drag $N(\sigma(\hat{u}))$ from a cG(1)cG(1) solution $\hat{U}=(U, P)$ using the formula

$$N^h(\sigma(\hat{U})) = \frac{1}{|I|}\int_I (\dot{U}+U\cdot\nabla U - f, \Phi) - (P, \nabla\cdot\Phi) + (2\nu\varepsilon(U), \varepsilon(\Phi)) + (\nabla\cdot U, \Theta) + \mathrm{SD}_\delta(U, P; \Phi, \Theta)\,\mathrm{d}t \tag{6}$$

where now Φ and Θ are finite element functions (with as before $\Phi=\phi$ on Γ_0 and $\Phi=0$ on Γ_1), and where $\dot{U}=(U^n-U^{n-1})/k_n$ on I_n. We note the presence of the stabilizing term SD_δ in (6), compared with (5), which is added in order to obtain the independence of $N^h(\sigma(\hat{U}))$ from the choice of (Φ, Θ), given by (4).

5. AN ADAPTIVE ALGORITHM

We introduce the following dual problem: Find $\hat{\varphi}=(\varphi, \theta)$ with $\varphi=\Phi$ on Γ_0 and $\varphi=0$ on Γ_1, such that

$$\begin{aligned} -\dot{\varphi} - (u\cdot\nabla)\varphi + \nabla U\cdot\varphi - \nu\Delta\varphi + \nabla\theta = 0 \quad &\text{in } \Omega\times I \\ \nabla\cdot\varphi = 0 \quad &\text{in } \Omega\times I \\ \varphi(\cdot, T) = 0 \quad &\text{in } \Omega \end{aligned} \tag{7}$$

where $(\nabla U\cdot\varphi)_j=(U)_{,j}\cdot\varphi$.

Replacing the exact dual solution $\hat{\varphi}$ by a computed approximation $\hat{\varphi}_h=(\varphi_h, \theta_h)$, we are led to the following *a posteriori* output error estimate [3, 9, 10], assuming sufficient regularity of $\hat{\varphi}_h$:

$$|N(\sigma(\hat{u})) - N^h(\sigma(\hat{U}))| \approx \left|\sum_{K\in\mathscr{T}} \mathscr{E}_{K,h}\right| \tag{8}$$

where $\mathscr{E}_{K,h}=e^K_{\mathrm{D},h}+e^K_{M,h}$ is an error indicator for element K in the mesh $\mathscr{T}$, and

$$\begin{aligned} e^K_{\mathrm{D},h} &= \frac{1}{|I|}\int_I ((|R_1(U,P)|_K + |R_2(U,P)|_K)\cdot(C_h h^2|D^2\varphi_h|_K + C_k k|\dot{\varphi}_h|_K) \\ &\quad + \|R_3(U)\|_K\cdot(C_h h^2\|D^2\theta_h\|_K + C_k k\|\dot{\theta}_h\|_K))\,\mathrm{d}t \\ e^K_{M,h} &= \frac{1}{|I|}\int_I |\mathrm{SD}_\delta(U, P; \varphi_h, \theta_h)_K|\,\mathrm{d}t \end{aligned}$$

where we may view $e^K_{\mathrm{D},h}$ as an error contribution from the Galerkin part of the cG(1)cG(1) discretization, and $e^K_{M,h}$ a contribution from the stabilization in cG(1)cG(1) on element K, and k

DOI: 10.1002/fld

and h are the time step and the local mesh size, respectively. The residuals R_i are defined by

$$\begin{aligned} R_1(U,P) &= \dot{U} + U\cdot\nabla U + \nabla P - f - \nu\Delta U \\ R_2(U,P) &= \nu D_2(U) \\ R_3(U,P) &= \nabla\cdot U \end{aligned} \tag{9}$$

with

$$D_2(U)(x,t) = \max_{y\in\partial K} (h_n(x))^{-1} \left| \left[\frac{\partial U}{\partial n}(y,t) \right] \right| \tag{10}$$

for $x \in K$, with $[\cdot]$ the jump across the element edge ∂K. D^2 denotes second-order spatial derivatives, and we write $|w|_K \equiv (\|w_1\|_K, \|w_2\|_K, \|w_3\|_K)$ with $\|w\|_K = (w,w)_K^{1/2}$, and let the dot denote the scalar product in $\mathbb{R}^3$.

Here $R_1(U,P)$ is defined elementwise, and with piecewise linears in space the Laplacian ΔU is zero. We have that $R_1(U,P)+R_2(U,P)$ bounds the residual of the momentum equation, with the Laplacian term bounded by the second-order difference quotient $D_2(U)$ arising from the jumps of normal derivatives across element boundaries. In the computations, we use $C_k = \frac{1}{2}$ and $C_h = \frac{1}{8}$ as constant approximations of the interpolation constants in (8), where these values are motivated by simple analysis on reference elements. Non-Dirichlet boundary conditions, such as slip conditions at lateral boundaries and transparent outflow conditions, introduce additional boundary terms in the *a posteriori* error estimate (8). But since the dual solutions for the problem in this paper are small at such non-Dirichlet boundaries, we neglect the corresponding boundary terms in (8).

The dual problem (7) is a linear convection–diffusion–reaction problem where the convection acts backward in time and in the opposite direction of the exact flow velocity u. The coefficient ∇U of the reaction term is locally large in turbulent regions, and thus potentially generating rapid exponential growth. However, ∇U is fluctuating, and the net effect of the reaction term with respect to drag in this paper turns out to generate slower growth, as we learn from computing approximations of the dual solution. We have the same experience from computing dual solutions related to mean value output in other turbulent flow problems [3, 9, 10], where we find that the dual solution is stable under perturbations, and thus (8) can be trusted even if we have errors in $\hat{\varphi}_h$ from computational approximation, and from linearizing at the approximate convection velocity U instead of the exact velocity u.

In this paper, we keep the space mesh $\mathcal{T}$ and time step k constant in time, with the time step being equal to the smallest element diameter in the space mesh, and we use an algorithm for adaptive mesh refinement in space, based on the *a posteriori* error estimate (8), for the approximation of mean drag, of the form:

Given an initial coarse computational space mesh $\mathcal{T}^0$, start at $k=0$, then

(1) Compute approximation of the primal problem using $\mathcal{T}^k$.
(2) Compute approximation of the dual problem using $\mathcal{T}^k$.
(3) If $|\sum_{K\in\mathcal{T}^k} \mathcal{E}^k_{K,h}| <$ TOL then STOP, else:
(4) Refine a fraction of the elements in $\mathcal{T}^k$ with largest $\mathcal{E}^k_{K,h} \to \mathcal{T}^{k+1}$.
(5) Set $k=k+1$, then goto (1).

DOI: 10.1002/fld

6. COMPUTATIONAL MODEL

We consider the flow past a circular cylinder of diameter D and length $4D$, with the cylinder in the direction of the x_3-axis, subject to a unit streamwise velocity inflow condition (in the x_1-direction) in a channel of length $21D$, width $4D$, and height $14D$. We use no-slip boundary conditions on the cylinder, slip boundary conditions on the lateral walls of the channel, and a transparent outflow boundary condition [3] at the end of the channel. We consider the cases of $Re=100$ and 3900, with the Reynolds numbers being based on the cylinder diameter D.

In this paper we want to compute the drag coefficient c_{D}, defined as a global average of a normalized drag force on the cylinder from the flow. We seek to approximate c_{D} by $\bar{c}_{\mathrm{D}}$, a normalized drag force averaged over a finite time interval $I=[0, 35D/U_\infty]$ at fully developed flow, defined by

$$\bar{c}_{\mathrm{D}} \equiv \frac{1}{\frac{1}{2}U_\infty^2 A} \times N(\sigma(\hat{u})) \tag{11}$$

where $U_\infty=1$ is the inflow velocity, $A=D\times 4D=4D^2$ is the cylinder area facing the mean flow, and $N(\sigma(\hat{u}))$ is defined in (5). In computations, we approximate $\bar{c}_{\mathrm{D}}$ by $\bar{c}_{\mathrm{D}}^h$ defined by

$$\bar{c}_{\mathrm{D}}^h = \frac{1}{\frac{1}{2}U_\infty^2 A} \times N^h(\sigma(\hat{U})) \tag{12}$$

with $N^h(\sigma(\hat{U}))$ being defined by (6). Thus, we may use a scaled version of the *a posteriori* error estimate (8) to estimate the error $|\bar{c}_{\mathrm{D}}-\bar{c}_{\mathrm{D}}^h|$.

7. COMPARISON WITH EXPERIMENTAL DATA

The flow past a circular cylinder is a well-documented problem, with many experimental reference values available. The reference results in this section are taken from [1, 2, 5–7] and references therein. Approximate solutions using G2 are plotted in Figures 1 and 2, where we observe vortex shedding, and for $Re=3900$ a large turbulent wake attached to the cylinder.

In Figure 3, we plot computational approximations of the drag coefficient, as we refine the mesh. For $Re=100$ we have convergence to $\bar{c}_{\mathrm{D}}^h\approx 1.47$ for the finest mesh, a value that is more or less constant for all meshes with more than 26 624 nodes, and this value for the drag coefficient is within the experimental tolerance. For $Re=3900$, we have $\bar{c}_{\mathrm{D}}^h\approx 0.97$ for the finest mesh, and we note that $\bar{c}_{\mathrm{D}}^h$ is within the experimental tolerance $c_{\mathrm{D}}=0.98\pm 0.05$ for all meshes using more than 28 831 nodes in the mesh. We are also able to capture the correct Strouhal numbers, with $St=0.16$ for $Re=100$ and $St\approx 0.22$ for $Re=3900$.

For circular cylinders, it is common to study the mean surface pressure on the cylinder as a function of an angle starting from the stagnation point at the leading edge of the cylinder. We define the *pressure coefficient* c_p by

$$c_p = \frac{p-p_\infty}{\frac{1}{2}U_\infty^2} \tag{13}$$

DOI: 10.1002/fld

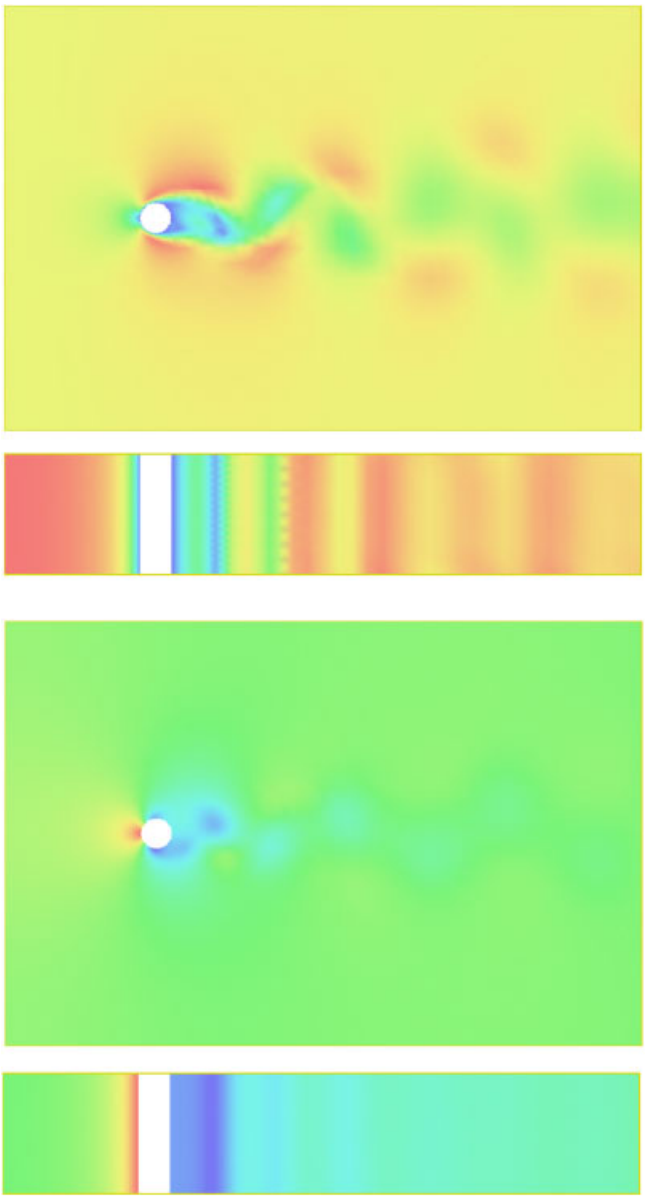

Figure 1. $Re = 100$: magnitude of velocity $|U|$ (upper) and pressure P (lower) in the midsections of the x_1x_2- and x_1x_3-planes, respectively.

where p is averaged in time and in the x_3-direction, and where U_∞ and p_∞ are the *free stream velocity* and the *free stream pressure*, respectively. In Figure 4 we plot the pressure coefficients, both matching experimental results, with a *base pressure coefficient* $C_{P_b} = -0.71$ for $Re = 100$ and $C_{P_b} = -0.90$ for $Re = 3900$.

DOI: 10.1002/fld

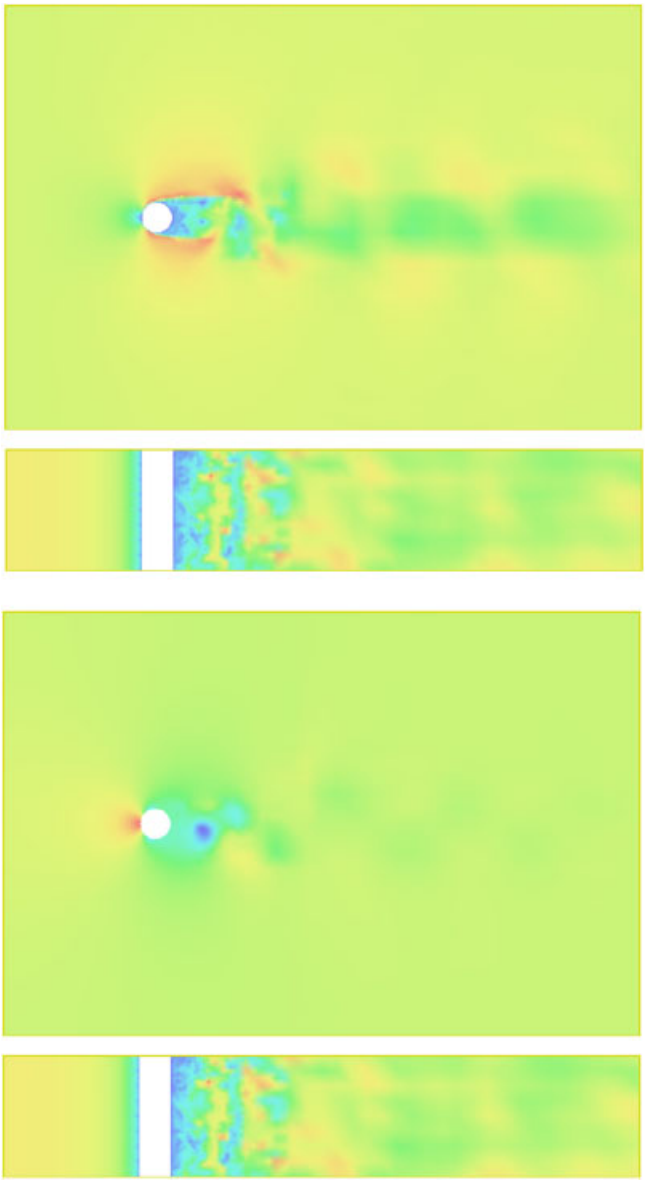

Figure 2. $Re = 3900$: magnitude of velocity $|U|$ (upper) and pressure P (lower) in the midsections of the x_1x_2- and x_1x_3-planes, respectively.

8. COMPARISON WITH LES COMPUTATIONS

The idea of G2 is to compute a certain output to a given tolerance, using a minimal number of degrees of freedom. We are thus interested in comparing the number of mesh points needed in G2

DOI: 10.1002/fld

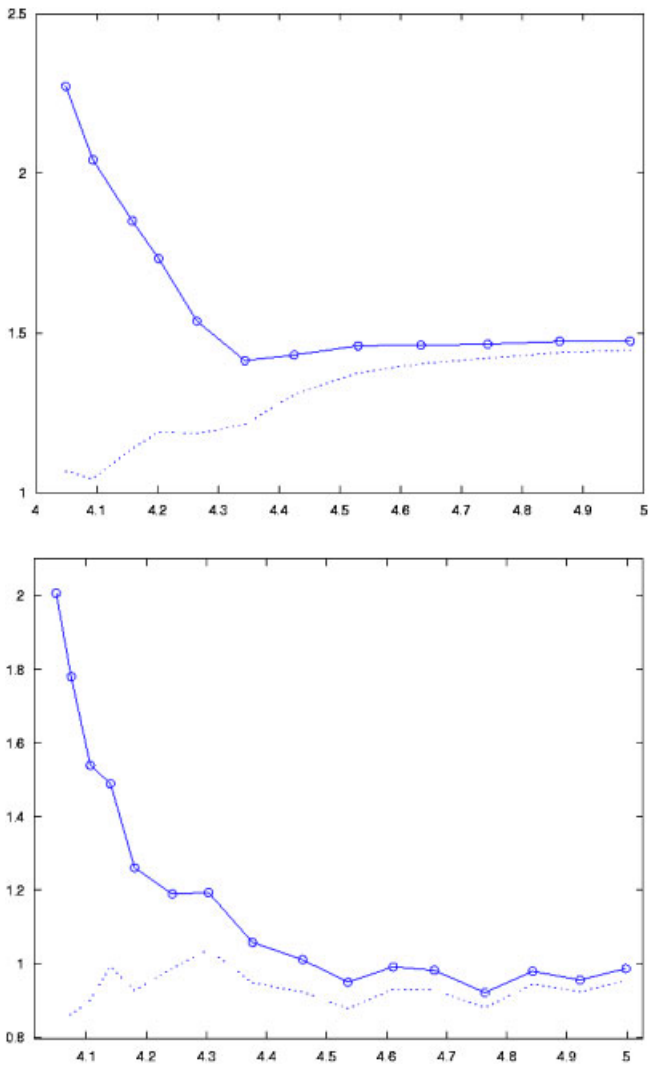

Figure 3. Approximate drag coefficient $\bar{c}_{\mathrm{D}}^{h}$ as a function of the 10-logarithm of the number of mesh points in space with ('o') and without (':') the stabilizing term in (6), for $Re = 100$ (upper) and $Re = 3900$ (lower).

to compute a certain output, compared with other approaches. Using less than 10^5 mesh points in space, we are able to capture the correct c_{D}, c_p, $C_{P_{\mathrm{b}}}$, and St, and using less than 30 000 mesh points we are able to capture c_{D} within the experimental tolerance.

In [5–7] LES is used to simulate flow past a circular cylinder at $Re = 3900$, using various numerical methods, subgrid models, and computational meshes. The mesh in [7] is of size $401 \times 120 \times 48$, and the results are within the experimental tolerances, and in [5] results for a mesh with 1 333 472 mesh points are presented, also within the experimental tolerances. In [6] various

DOI: 10.1002/fld

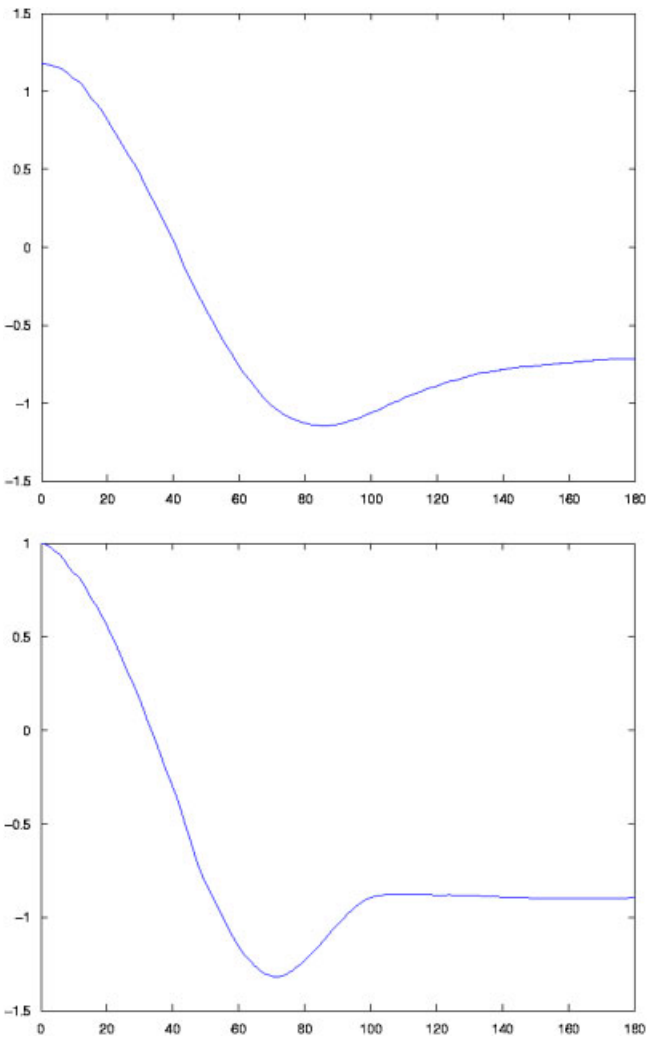

Figure 4. Pressure coefficient c_p as a function of an angle starting at the stagnation point, for $Re = 100$ (upper) and $Re = 3900$ (lower).

numerical methods and subgrid models are used for meshes of size $165 \times 165 \times 32$, $165 \times 165 \times 64$, and $209 \times 165 \times 32$, with some results within the experimental tolerance, but others not, depending on the subgrid models and the numerical methods used.

9. DUAL SOLUTION AND *A POSTERIORI* ERROR ESTIMATES

The solution to the dual problem contains information of how local errors influence the error in the output of interest. In the *a posteriori* error estimate (8), the error in mean drag is estimated in terms

DOI: 10.1002/fld

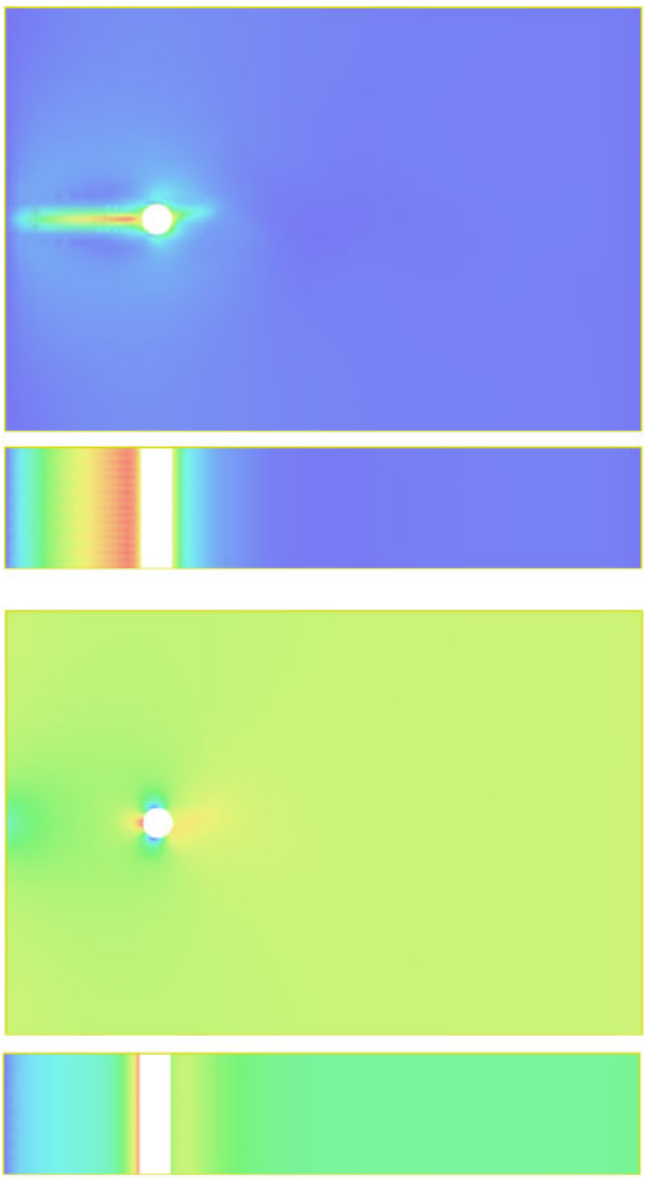

Figure 5. $Re = 100$: magnitude of dual velocity $|\varphi_h|$ (upper) and dual pressure $|\theta_h|$ (lower) in the midsections of the x_1x_2- and x_1x_3-planes, respectively.

of residuals, measuring the local error, weighted by derivatives of the dual solution, measuring the influence of the non-zero residuals on the error in mean drag.

The data in the dual problem are given by the output of interest, with a mean value output corresponding to regular data, and more local output corresponding to more irregular data. For computation of mean drag, the data to the dual problem are constant boundary conditions on the

DOI: 10.1002/fld

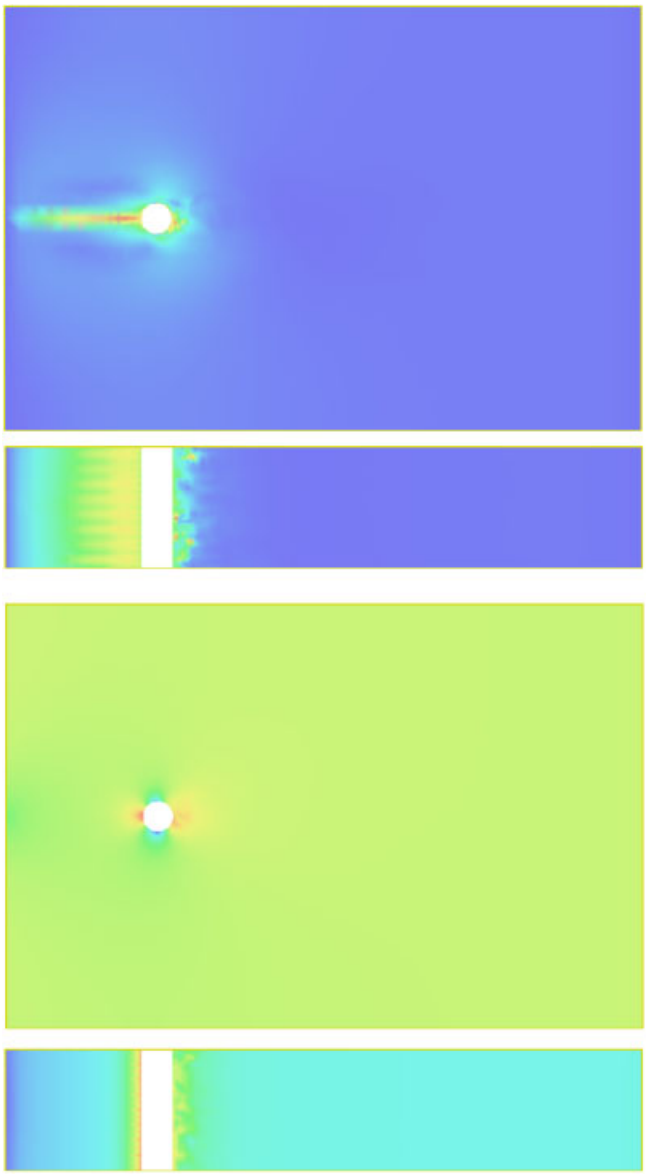

Figure 6. $Re = 3900$: magnitude of dual velocity $|\varphi_h|$ (upper) and dual pressure $|\theta_h|$ (lower) in the midsections of the x_1x_2- and x_1x_3-planes, respectively.

cylinder of a unit vector in the streamwise direction, and the dual solution gives the information of what part of the computational domain is important for accurate approximation of mean drag.

In Figures 5 and 6, we plot snapshots of the dual solutions corresponding to approximation of mean drag for $Re = 100$ and 3900, and in Figure 7 we plot the resulting computational meshes. Studying the different meshes, we note that the mesh corresponding to $Re = 100$ is almost symmetric

DOI: 10.1002/fld

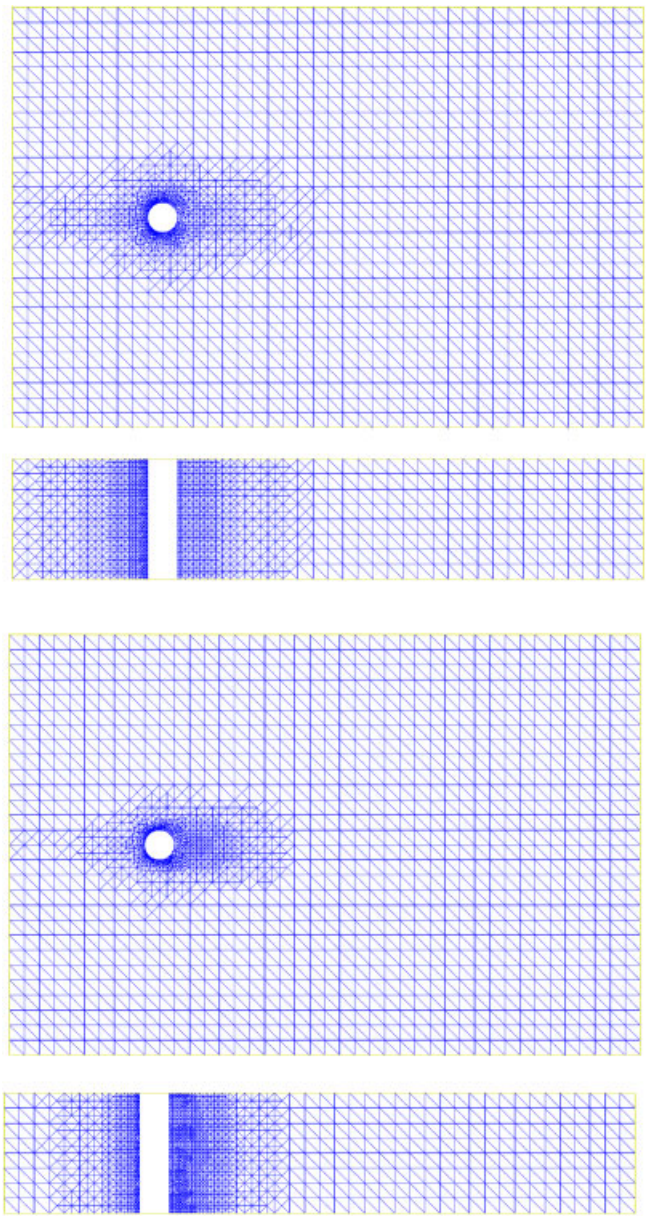

Figure 7. Meshes for $Re = 100$ (upper), and $Re = 3900$ (lower), in the midsections of the x_1x_2- and x_1x_3-planes respectively.

in the streamwise direction and that the mesh refinement is spread wider vertically for this laminar flow than for the turbulent flow corresponding to $Re = 3900$. For $Re = 3900$, the mesh refinement is concentrated to the boundary layer of the cylinder and to the turbulent wake. Overall, the mesh refinement is more localized for the higher Reynolds number, which is consistent with the dual

DOI: 10.1002/fld

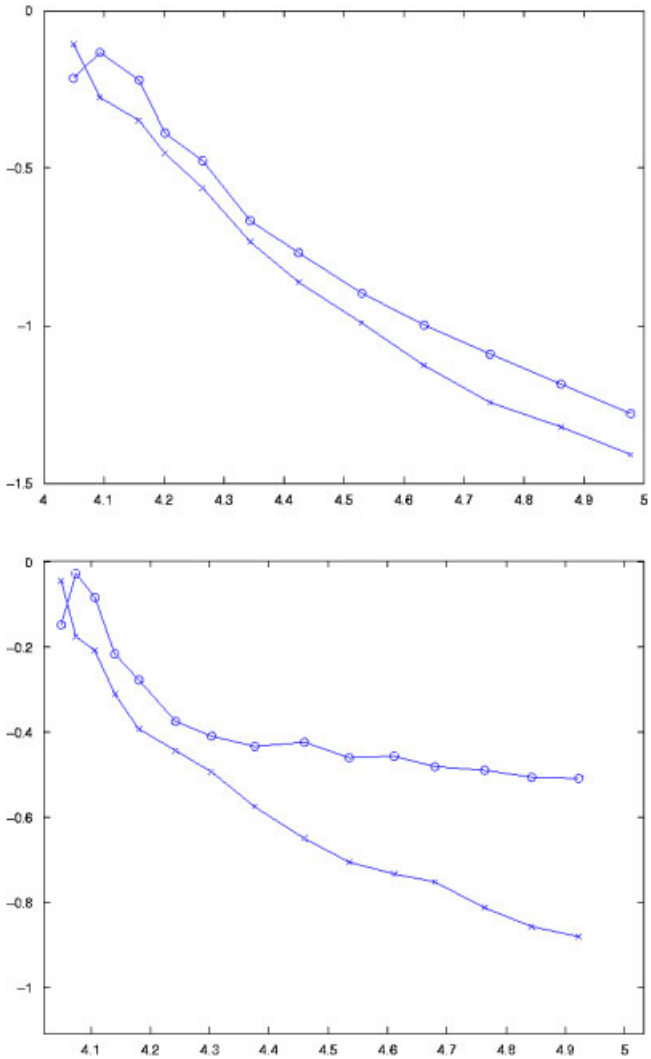

Figure 8. *A posteriori* error estimates from (8): $e_{\mathrm{D},h} = \sum_{K\in\mathscr{T}} e^K_{\mathrm{D},h}$ ('o') and $e_{M,h} = \sum_{K\in\mathscr{T}} e^K_{M,h}$ ('x') for $Re = 100$ (upper) and $Re = 3900$ (lower).

problem being convection dominated, whereas the dual problem for the lower Reynolds number is more viscous and thus spreads the data more.

In Figure 8 we plot *a posteriori* error estimates for c_{D}. We note that for the laminar flow at $Re = 100$, the convergence rate is high and we may expect to obtain a sharp bound on the error by further refining the mesh. For $Re = 3900$ the situation is different. We cannot expect to determine mean drag to an arbitrary small tolerance, due to the strong perturbation growth in a turbulent flow, with a highly fluctuating flow field. This connects the questions of uniqueness and computability of mean values in a turbulent flow [3].

DOI: 10.1002/fld

We can compare this with the problem of predicting the temperature in London, where we cannot expect to be able to predict the daily temperature on July 1 each year to a tolerance less than say $\pm 10^{\circ}$C, which is typically of no interest. On the other hand, we may be able to predict the monthly mean temperature of July to a tolerance of say $\pm 2^{\circ}$C, which is of interest, and which we find in a typical guide book for London.

But not even for the monthly mean value, we can expect to predict the temperature to an arbitrary small tolerance. The same is true for the approximation of c_{D} for a circular cylinder in a turbulent flow. We cannot expect the tolerance, in terms of the *a posteriori* error estimates, to be arbitrary small. Judging from experimental results, and the approximate values in Figure 3, a tolerance of about ± 0.05–0.1 for c_{D} seems reasonable, and thus the *a posteriori* error estimate in Figure 8 for the finest mesh would indicate an error that is about a factor 4–8 too large, which is similar to our experiences from other problems of the same type [3], where the overestimation of the output error results from taking absolute values in space and time, for example.

10. SUMMARY

We have shown that we are able to use G2 to compute the drag coefficient c_{D} for the turbulent flow past a circular cylinder at Reynolds number $Re = 3900$. We find that we are able to approximate c_{D} to an accuracy of a few percent, corresponding to the accuracy in experimental results, using less than 10^5 mesh points in space, which makes the simulations possible using a standard PC.

REFERENCES

1. Zdravkovich MM. *Flow Around Circular Cylinders*: *A Comprehensive Guide through Flow Phenomena*, *Experiments*, *Applications*, *Mathematical Models*, *and Simulations*, *Vol. 1*: *Fundamentals*. Oxford University Press: Oxford, 1997.
2. Schlichting H. *Boundary Layer Theory*. McGraw-Hill: New York, 1955.
3. Hoffman J, Johnson C. *Computational Turbulent Incompressible Flow*: *Applied Mathematics Body and Soul*, vol. 4. Springer: Berlin, 2007.
4. Sagaut P. *Large Eddy Simulation for Incompressible Flows*. Springer: Berlin, Heidelberg, New York, 2001.
5. Kravchenko AG, Moin P. Numerical studies of flow over a circular cylinder at $Re_d = 3900$. *Physics of Fluids* 2000; **12**(2):403–417.
6. Breuer M. Large eddy simulation of the subcritical flow past a circular cylinder: numerical and modeling aspects. *International Journal for Numerical Methods in Fluids* 1998; **28**:1281–1302.
7. Mittal R. Progress on LES of flow past a circular cylinder. *Annual Research Briefs*, Center for Turbulence Research, 1996.
8. Dunca A, John V, Layton WJ. The commutation error of the space averaged Navier–Stokes equations on a bounded domain. In *Contributions to Current Challenges in Mathematical Fluid Mechanics*, Galdi GP, Heywood JG, Rannacher R (eds). Advances in Mathematical Fluid Mechanics, vol. 3. Birkhäuser: Basel, 2004; 53–78.
9. Hoffman J, Johnson C. A new approach to computational turbulence modeling. *Computer Methods in Applied Mechanics and Engineering* 2006; **195**:2865–2880.
10. Hoffman J. Computation of mean drag for bluff body problems using adaptive DNS/LES. *SIAM Journal on Scientific Computing* 2005; **27**(1):184–207.
11. Eriksson K, Estep D, Hansbo P, Johnson C. Introduction to adaptive methods for differential equations. *Acta Numerica* 1995; **4**:105–158.
12. Becker R, Rannacher R. A posteriori error estimation in finite element methods. *Acta Numerica* 2001; **10**:1–103.
13. Giles M, Süli E. Adjoint methods for PDEs: a posteriori error analysis and postprocessing by duality. *Acta Numerica* 2002; **11**:145–236.
14. Becker R, Rannacher R. A feed-back approach to error control in adaptive finite element methods: basic analysis and examples. *East-West Journal of Numerical Mathematics* 1996; **4**:237–264.

DOI: 10.1002/fld

15. Giles M, Larson M, Levenstam M, Süli D. Adaptive error control for finite element approximations of the lift and drag coefficients in viscous flow. *Technical Report NA-76/06*, Oxford University Computing Laboratory, 1997.
16. Hoffman J, Johnson C. Adaptive finite element methods for incompressible fluid flow. In *Error Estimation and Solution Adaptive Discretization in Computational Fluid Dynamics*, Barth TJ, Deconinck H (eds). Lecture Notes in Computational Science and Engineering. Springer: Heidelberg, 2002; 97–158.
17. Hoffman J. On duality based a posteriori error estimation in various norms and linear functionals for LES. *SIAM Journal on Scientific Computing* 2004; **26**(1):178–195.

DOI: 10.1002/fld